Characterization Measurements Methodology and Instrumental Set-Up Optimization for New SiPM Detectors—Part II: Optical Tests

Giovanni Bonanno, Davide Marano, Massimiliano Belluso, Sergio Billotta, Alessandro Grillo, Salvatore Garozzo, Giuseppe Romeo, and Maria Cristina Timpanaro

***Abstract*— A comprehensive and in-depth characterization procedure for obtaining very accurate measurements on silicon photomultiplier detectors (SiPMs) is here described. A large amount of optical tests are systematically carried out and discussed in terms of the most important SiPM performance parameters; in particular, an accurate estimation of the photon detection efficiency in the 350–900-nm wavelength spectral range and in steps of 10 nm is achieved, based on the single-photon counting technique, with substraction of the dark noise contribution and avoiding the additional noise sources of crosstalk and afterpulsing. Some recently produced detectors are analyzed and their relevant electro-optical parameters are evaluated in order to demonstrate the effectiveness and efficacy of the adopted characterization procedure and data-handling protocols in assessing the overall SiPM performance, regardless of the specific device tested. Tests repeatability is carefully verified and all the evaluated parameter trends are proved to be compatible with the physics theory of the SiPM device.**

***Index Terms*— Electro-optical characterizations, precision measurements, silicon photomultipliers, solid-state detectors.**

I. Introduction

IN LINE with the growing evolution of astrophysics, medical imaging and nuclear science, the realization of optical solid-state sensors has been given a continuously rising emphasis during the recent years and is gaining a significant and widespread research interest within the scientific community.

Silicon Photo-Multiplier detectors (SiPMs), also referred to as Multi-Pixel Photon Counters (MPPCs), are a relatively new category of semiconductor device addressing the challenge of detecting, timing and quantifying low-light signals down to the single-photon level. SiPM sensors operate at low bias voltages and feature a high multiplication ratio, fast dynamic response, excellent time resolution, high photon detection efficiency and wide spectral response range; as a consequence, they are capable of delivering the high-performance level required for photon counting applications and thus have a strong inherent potential for replacing traditional phototube detectors.

The number of perspective applications exploiting the advantages of SiPMs is rapidly increasing over time, and remarkable research studies and technological development in this class of detectors have been extensively undertaken by a rising number of companies and institutions [1]–[21].

SiPM detectors promise to fulfill a wide set of requirements coming from a large number of emerging contexts, and several silicon foundries primarily driven by the physical and medical fields are currently investing in future development and innovation. Recently, new SiPM detectors with enhanced overall features have been produced by the world leading manufacturers, and further performance improvements are shortly foreseen.

For a particular application field, an appropriate experimental set-up and a well-defined characterization procedure for SiPM sensors is important to explain how accurate measurements and systematic data-handling procedures for the evaluation of their electro-optical parameters can be profitably exploited to obtain a reliable qualification of the detector performance.

The systematic procedures pursued to derive the major SiPM performace parameters, along with the extensive analyses and measurements performed on different devices, have allowed for a standardization of the adopted testing methodology, in order to be profitably applicable to every kind of solid-state detectors produced by all manufacturing industries.

The present part of the manuscript is focussed on the optical characterization of SiPM detectors, in terms of dark count rate assessment, cross-talk analysis and estimation, optical dynamic range tests and measurements, and photon detection efficiency evaluation, and represents the natural and subsequent complement of the work performed in the previous part, devoted to the initial SiPM electrical analysis and characterization.

It should be remarked that all PDE measurements carried out and presented are treated so as to reduce as much as possible the contributions of cross-talk and afterpulsing, allowing a reliable determination of the detector optical performance.

II. Set-Up Environment

The experimental equipment set-up exploited for the optical characterizations of solid-state detectors is one of the available

Manuscript received November 6, 2013; revised April 22, 2014; accepted May 30, 2014. Date of publication June 4, 2014; date of current version August 29, 2014. The associate editor coordinating the review of this paper and approving it for publication was Prof. Alexander Fish.

The authors are with the Istituto Nazionale di Astrofisica, Osservatorio Astrofisico di Catania, Catania I-95123, Italy (e-mail: giovanni.bonanno@oact.inaf.it; davide.marano@oact.inaf.it; massimiliano.belluso@oact.inaf.it; sergio.billotta@oact.inaf.it; alessandro.grillo@oact.inaf.it; salvatore.garozzo@oact.inaf.it; giuseppe.romeo@oact.inaf.it; mc.timpanaro@oact.inaf.it).

Color versions of one or more of the figures in this paper are available online at http://ieeexplore.ieee.org.

Digital Object Identifier 10.1109/JSEN.2014.2328623

1530-437X © 2014 IEEE. Personal use is permitted, but republication/redistribution requires IEEE permission.
See http://www.ieee.org/publications_standards/publications/rights/index.html for more information.

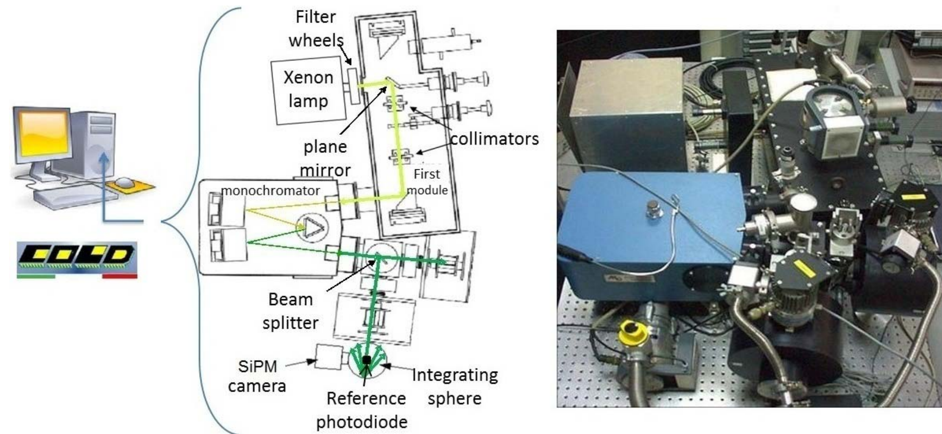

Fig. 1. Simplified schematization of the COLD optical apparatus. On the right side: photograph of the characterization equipment. On the left side: scheme of the implemented mechanical and optical parts of the apparatus, where the green line indicates the light path.

facilities at the Catania astrophysical Observatory Laboratory for Detectors (COLD). It is a long time since COLD laboratory is concerned with detectors characterization [10]. In the recent past various photon counting devices have been characterized, such as SPADs, SPAD arrays, and first generation SiPMs [10]–[15]. A detailed description of the initial optical equipment can be found in [12]. For each detector an appropriate instrumental apparatus, tailored for the specific device, has been employed. The optical apparatus of the characterization facility has been slightly modified from the original realization.

In the following, a brief description of the novel testing environment engaged for the optical characterization is addressed.

A. Instrumental Equipment

The experimental set-up adopted is partially based on optical systems, such as light sources, precision filters, monochromator and integrating sphere, and partially based on particle counting equipment. The main instruments involved in the set-up are:

- The COLD optical apparatus;
- A Keithley 6514 femtoammeter;
- A CAEN SP5600 PSAU unit;
- A Tektronix FCA3000 frequency counter;
- A CAEN V1290 time-to-digital converter.

The COLD optical equipment, developed at "INAF Osservatorio Astrofisico di Catania" and used for the optical detectors characterization, is illustrated in Fig. 1. A Xenon lamp is used as a radiation source; a wavelength selection system constituted by a set of band-pass filters and mirrors, and a Czerny-Turner monochromator are exploited to achieve the desired wavelength in the 130-1100nm spectral range, with a FWHM smaller than 1nm. A beam splitter is employed to direct the monochromatic radiation through an optical lens towards an integrating sphere, which hosts, in one port, a 1-cm^2 NIST-traced reference photodiode along with the SiPM sensor to be characterized.

The photon flux intensity coming into the integrating sphere can be regulated by means of neutral density filters or changing the aperture of the entrance or exit slits of the monochromator. Due to the small dimensions of the detectors to be characterized with respect to the optical beam, the integrating sphere is used to spatially integrate the radiant flux. Furthermore, appropriate mechanical structures are realized, in terms of both aperture and distance from the centre of the sphere, to illuminate the SiPM detector and the NIST-traced photodiode with the same radiant flux. The reference photodiode allows to evaluate the number of photons per unit area, and then, after a proper rescaling, the number of photons impinging on the detectors under test.

The Keithley ammeter is able to measure a current ranging from 20pA up to 20mA with a digital resolution of 0.1fA, and is programmable via a GPIB (IEEE 488) standard interface.

The CAEN V1290 is a 16-channel time-to-digital converter featuring a LSB of 25ps (21-bit resolution, 52-µs FSR) and can be readout and programmed via VME. The module is inserted in a VME crate, connected to a PC by means of a fiber optic.

The CAEN power supply amplification unit (PSAU) and the Tektronix counter are described in the first part of the paper.

B. Experimental Set-Up

In this subsection, the apparatus setups for the SiPM optical characterization measurements are described.

The experimental set-up used for photon detection efficiency (PDE) measurements is sketched in Fig. 2.

Before starting the final PDE tests, the appropriate discriminator threshold must be selected to catch the SiPM pulses. For this purpose, the section of the PDE apparatus enclosed in the red-dashed box in Fig. 2 is exploited to trace the staircase plots, allowing to select the appropriate threshold to be used for the PDE measurements and evaluate the crosstalk contribution.

During staircase measurements, SiPMs are kept in dark. Due to the different behavior of the tested detectors, two different set-up systems can be employed for the stairs tests, for which the CAEN PSAU is used, in both cases, as a power supply and amplifier for the SiPM sensor.

If the detector is affected by extra-charge noise, the PSAU is also adopted as a discriminator and counter for the SiPM output signal. The software implemented to control the PSAU allows to automatically change the discriminator threshold and acquire the relevant counts. At the end of the procedure,

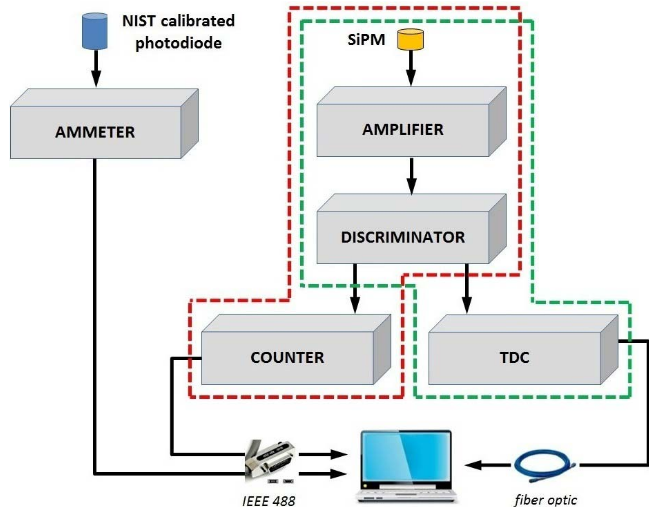

Fig. 2. Schematic overview of the experimental apparatus set-up implemented for dark staircase (red-dashed box), extra-charge (green-dashed box) and photon detection efficiency (whole system) measurements.

the measured counts are plotted as a function of the threshold voltage.

On the other hand, if the detector has no extra-charge effects, the SiPM amplified output from the PSAU system is fed into the Tektronix counter. As in the previous case, a specific software interface allows to automatically vary the discriminator threshold inside the counter and acquire the relevant counts. At the end of the procedure, thresholds and counts are saved into a file to be plotted by an electronic spreadsheet.

Once the optimal threshold is established, the PSAU digital output is connected to the CAEN TDC (as shown in the section delimited by the green-dashed line in Fig. 2) to assess the extra-charge noise. The software realized to control the CAEN TDC allows to acquire and save each recorded time tag. The data can be analyzed to reconstruct a histogram of the number of events as a function of the time interval between two adjacent pulses, and evaluate the presence of extra-charge noise.

Final PDE measurements involve the exploitation of the full apparatus in Fig. 2, where the SiPM detector and the reference photodiode are mounted together onto the integrating sphere to be illuminated with a monochromatic light.

If the SiPM is affected by extra-charge, the digital output of the PSAU unit is connected to the Tektronix counter. The width of the digital pulse, which acts as a variable hold-off time, can be adjusted so as to suppress noise effects as much as possible. On the contrary, if no extra-charge occurs, the amplified SiPM signal from the PSAU is directly attached to Tektronix counter.

PDE tests are performed based on the measured SiPM count rate due to the real photo-events compared to the photocurrent signal measured by the ammeter (properly converted into number of electrons per second). The software realized for the PDE measurements allows to select a wavelength in the range of 130-1100nm and acquire the photocurrent by the Keithley ammeter and, simultaneously, the number of counts from the Tektronix counter. All wavelength, count and current data are saved into a file for a later analysis.

Tests are performed adjusting the photon flux level such that the reference diode is still sensitive and the SiPM detectors are safely in the single-photon regime with negligible pile-up.

Moreover, the introduction of a neutral density filter in front of the SiPM allows to operate at sufficiently high current levels on the calibrated photodiode to avoid low signal measurements and hence achieve a reduction in the experimental error bars.

It should be remarked that absolute PDE measures are here perfomed, since the adopted set-up configuration uses a certified calibrated photodiode to determine the absolute amount of light reaching the SiPMs. Furthermore, the adopted monochromator, in conjunction with the integrating sphere, allows PDE measurements over a wide spectral range, in steps of 10nm, and for very low detector dimensions (even smaller than 50μm).

III. Optical Characterization

In this section the adopted testing methodology for achieving reliable optical characterization measures is discussed. In particular, the reader is introduced into an important aspect to be consedered when evaluating the photon detection efficiency of the SiPM detectors with high accuracy levels. The requirement of having a well-defined methodology, accounting not only for the precision of all involved instruments, but also for the implemented procedure, is crucial to obtain accurate measurements.

Prior to the final PDE tests, some key parameters have to be arranged on the control electronics and optical set-up. Initially, the optimal threshold voltage is determined from the dark count rate measurements. Subsequently, the optimal hold-off time is established to avoid extra charge measurements. In addition, the illumination level at the output ports of the integrating sphere is adjusted to prevent photon rate impinging on the detector with consequent pile-up conditions and saturation. Finally, the photocurrent detected by the calibrated photodiode is controlled to avoid low-level signal measurements. Any inaccurate selection of the above parameters can result in severe PDE degradation.

Due to the intrinsic complexity of the detector under test and to the measurement set-up implemented, a brief schematization of the characterization activity performed is dutiful. The procedure steps of the systematic methodology envisaged to achieve accurate optical characterizations are listed below:

- Dark count stairs measurements, to establish the optimal threshold signal level;
- Dark count rate vs. gate time measurements, to establish the optimal hold-off time;
- Linearity measurements vs. photon rate, to avoid saturation and pile-up effects;
- Photon detection efficiency measurements for a specific overvoltage, and relevant comparisons;
- Photon detection efficiency measurements for a specific temperature, and relevant comparisons;
- Cross-talk and dark count rate assessment vs. overvoltage and temperature.

The adopted optical characterization procedure for the SiPM sensors is illustrated in Fig. 3 in a flow-chart form.

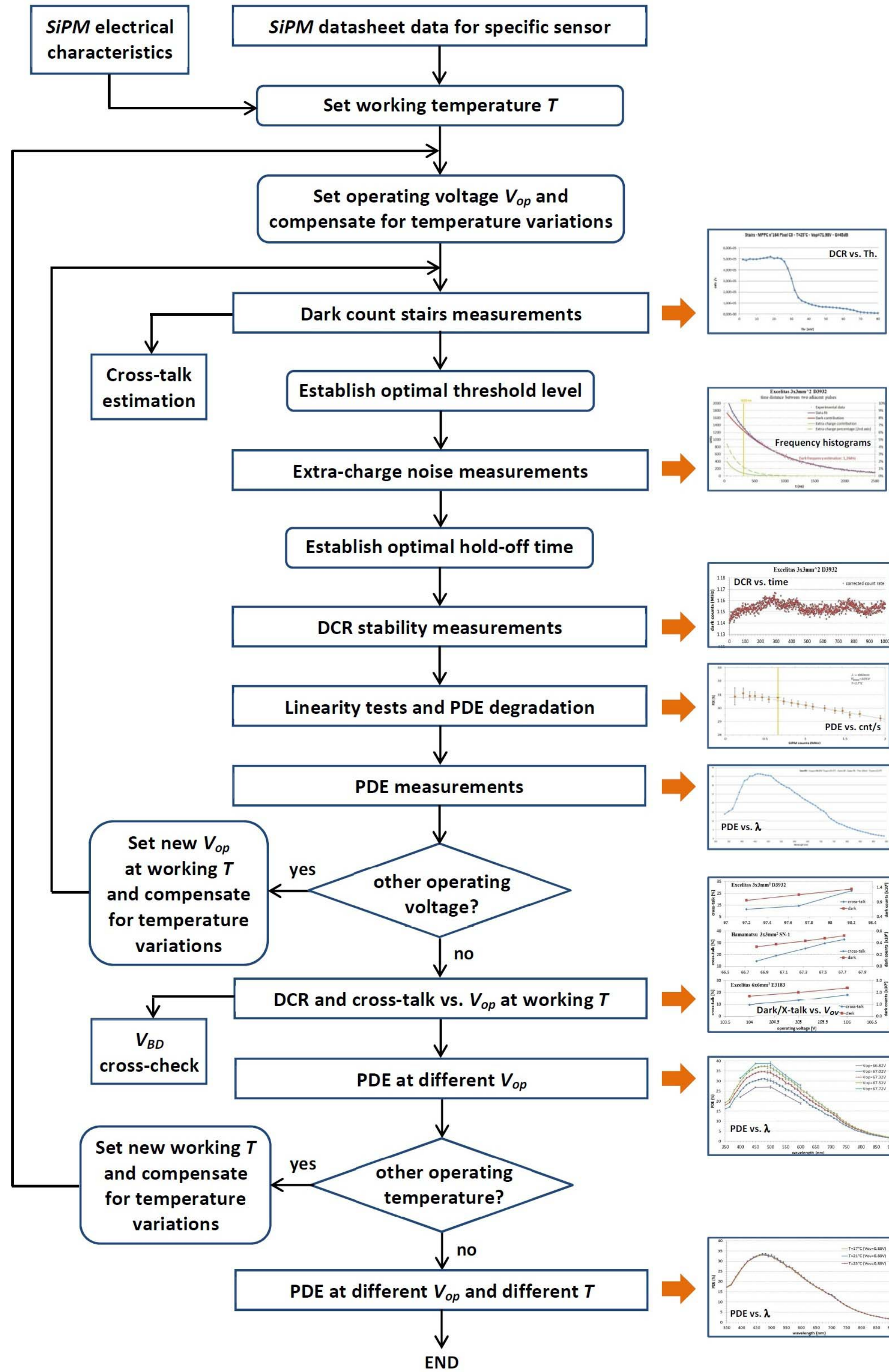

Fig. 3. Basic flow-chart representation of the adopted optical characterization procedure for SiPM detectors.

The SiPM devices referenced throughout the section include some recently produced prototypes by different manufacturers which have been sent to our laboratories for testing and evaluation purposes (and thus are not commercially available), whose main basic features are summarized in Table I.

A. Dark Count Stairs Measurements

The dark current is one of the crucial parameters affecting the performance of SiPM detectors. The noise figure for a Geiger-mode photosensor is identified with the dark count rate (DCR), defined as the number of avalanche current pulses produced by thermally generated carriers simulating the detection of single photons at a certain bias voltage.

Since the dark noise is comprised of a series of time pulses, its magnitude is often quoted as a pulse rate, typically expressed in kHz or MHz; however, for continuous or current integration measurements, it may be generally more convenient to consider the noise contribution as a dark current, expressed in μA.

TABLE I
MAIN FEATURES OF THE TESTED SIPM DEVICES

	Excelitas D3932 (*C30742-33-050C*)	Hamamatsu SN-1 (*S12572-050C*)	Excelitas E3183 (*C30742-66-050C*)
Active area	3.0×3.0 mm^2	3.0×3.0 mm^2	6.0×6.0 mm^2
Microcells	3600	3600	14400
Pixel pitch	50 μm	50 μm	50 μm
Fill factor	51.0 %	61.5 %	40.0 %

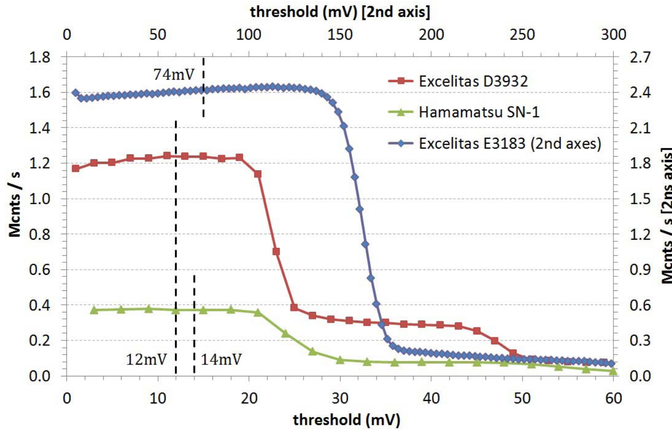

Fig. 4. Dark staircase functions for the three analyzed detectors and relevant 0.5-pe thresholds determination.

SiPM DCR is affected by the sensitive area of the photodetector (in terms of number and density of its sub-pixels), by the applied overvoltage V_{OV}, and by the operating temperature T.

A DCR scan plot of the three analyzed detectors for different values of the discriminator threshold V_{TH} is reported in Fig. 4. Characteristic step functions are observed, and the count rates sharply drop (typically by one order of magnitude in frequency) when integer multiples of a 1-photoelectron (pe) threshold are reached. For a threshold above the electronics noise and below the amplitude of 1-pe signal, all thermally generated excitations are counted, so that the corresponding measure provides a fair estimation of the SiPM dark rate. Such kinds of plots are often referred to as staircase functions or, simply, stairs.

The optimal threshold level for each device, also reported in Fig. 4, can be determined by the DCR measures at half-photon threshold, that is for a discriminator threshold corresponding to half the signal of the first photon pulse.

B. Dark Count Rate vs. Hold-Off Time Measurements

Photon counting resolution of SiPM devices may be affected by correlated extra-charge effects, resulting in additional pulse counts which are delayed with respect to the original avalanche discharges. Such excess noise effects may include afterpulsing and delayed or indirect optical cross-talk.

Afterpulsing is believed as being caused by the generation of false pulse counts arising from the emission of charge carriers, trapped in band-gap states within the depletion regions, during previous Geiger discharges; the trapped carriers eventually get

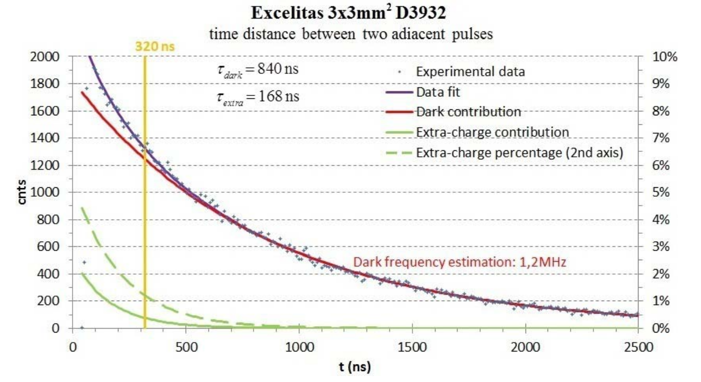

Fig. 5. Histograms of the time interval between two consecutive pulse signals and relevant fit curve for the Excelitas D3932 detector. The extra-charge noise contribution is represented by the continuous green line, and its percentage over the total number of events is shown by the green-dashed line. The low cut-off value of the fitted experimental data is 70 ns.

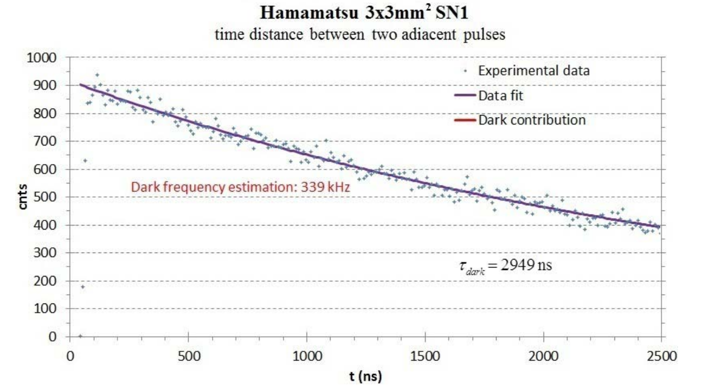

Fig. 6. Histograms of the time interval between two consecutive pulse signals relevant fit curve for the Hamamatsu SN-1 detector. The dark function and the fit curve are perfectly overlapped due to the absence of extra-charge noise. The low cut-off value of the fitted experimental data is 116 ns.

released and trigger delayed avalanches within the same pixels as the original discharges.

Delayed cross-talk occurs when secondary photons are able to produce additional electron-hole pairs close to neighboring microcells; the generated carriers can hence diffuse to the near sub-pixels and cause their delayed discharge. Similarly, indirect cross-talk is due to secondary photons, being reflected at one of the various device interfaces, that can reach a neighboring cell via multiple indirect paths.

Such extra-charge effects are hardly distinguished and result in an over-estimation of the SiPM detection efficiency.

To evaluate the amount and contribution of extra noise to the real signals, frequency histograms of the time intervals between two consecutive pulse signals are carried out for each detector under test. Fig. 5, Fig. 6 and Fig. 7 illustrate these distributions (blue dots) for the SiPMs in Table I. The measured values in the $0-2500$-ns region are fitted with a double exponential function (violet line), representing both dark (red line) and extra-charge (green line) contributions, whose expression is

$$f(t) = A_{\text{dark}} \exp\left(-\frac{t}{\tau_{\text{dark}}}\right) + A_{\text{extra}} \exp\left(-\frac{t}{\tau_{\text{extra}}}\right) \quad (1)$$

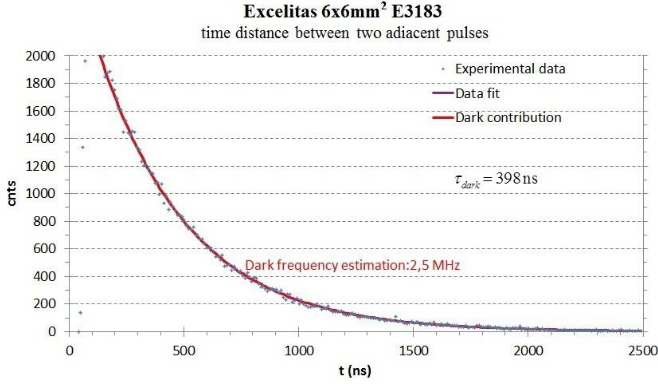

Fig. 7. Histograms of the time interval between two consecutive pulse signals relevant fit curve for the Excelitas E3183 detector. The dark function and the fit curve are perfectly overlapped due to the absence of extra-charge noise. The low cut-off value of the fitted experimental data is 90 ns.

where A_{dark} and A_{extra} are respectively the weights of the pure dark counts and extra-charge noise, whilst τ_{dark} and τ_{extra} are the time constants associated to the foregoing processes.

It is worth remarking that the above time constant τ_{extra} does not include the optical cross-talk generating signals equivalent to more than 1-pe avalanche events, as detailed in Section IIIE.

The fit functions obtained from the experimental data can be straightforwardly used to provide an immediate assessment of the dark count rate (represented by the reciprocal of parameter τ_{dark}), which can be checked against the relevant values measured by means of a direct counting. The close correspondence between the dark frequency values extracted by Figs. 5–7 (red labels) and the 0.5-pe DCR data of the same devices in Fig. 4 at the same operating conditions gives confidence on the correctness of the achieved results.

Referring to the distributions in Fig. 5, the green-dashed line represents the percentage of the extra-charge noise over the total number of events, from which it can be noted that extra-charge effects are observable as far as about 1μs. The vertical yellow line represents the maximum applicable hold-off time (320ns) resulting from the highest digital output width from the PSAU, at which the residual extra noise percentage is $\sim 1\%$.

On the other hand, for the SiPMs distributions in Figs. 6 and 7, the dark signals and the double-exponential fit curves are perfectly overlapped, due to the absence of extra-noise charge.

Thence, to reduce as much as possible (where necessary) the effects of extra-charge, a controlled hold-off time is eventually introduced by the measurement system for each detected pulse, and a statistical dead time correction is applied to account for the lost pulse signal. The dead time correction applied is based on the assumption that the arrival time of the incident photons is expected to follow a statistical Poissonian distribution, and is expressed by the following relationship

$$S_{corr} = \frac{S_0}{1 - t_{hold} S_0} \tag{2}$$

where S_0 stands for the number of counts per second, t_{hold} is the applied hold-off time, and S_{corr} is the corrected count rate.

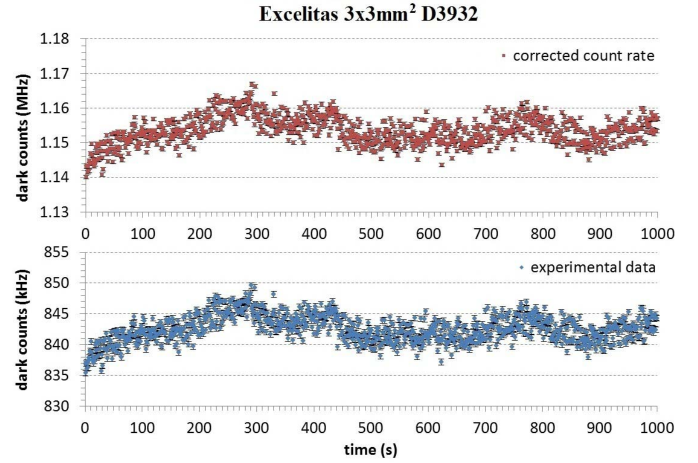

Fig. 8. Experimental (on bottom) and corrected (on top) DCR plots versus time for the Excelitas D3932 detector.

Fig. 8 illustrates the dark stability plots as a function of time for the Excelitas D3932 device, showing both experimental and corrected data in a 1000-s time interval. It can be inspected that the corrected DCR average value (upper plot) is consistent with the pure dark frequency estimation obtained from Fig. 5, for the same operating conditions.

By using this method, SiPM extra-charge noise can be characterized and taken into account in the right way; indeed, the threshold voltage can be set at a convenient value and the signal can be acquired with a given hold-off time (by varying the time length of the digital output pulse from the PSAU discriminator).

C. Instrumental Linearity Measurements

The photon detection operated by a SiPM sensor is a statistical process based on the probability of detecting stochastically distributed photons by the limited number of sensitive elements. Consequently, the total number of fired pixels does not directly correspond to the number of detected photons. If two or more photons are triggering the same diode microcell, then the photon detection linearity degrades because the number of incident photons is larger than the number of fired pixels.

For a light pulse shorter than the effective pixels dead time, the number of microcells fired, N_f, is a function of the number of incident photons and depends on the light source wavelength λ, on the applied overvoltage, and on the global number of pixel microcells N, and can be approximated by

$$N_f(N, V_{OV}, \lambda) = N\left\{1 - \exp\left[-\frac{N_{\text{det}}(V_{OV}, \lambda)}{N}\right]\right\} \tag{3}$$

where N_{det} is the effective number of detected photons, which is determined by the number of instantaneous incident photons, N_{ph}, and by the device photon detection efficiency

$$N_{\text{det}}(V_{OV}, \lambda) = PDE(V_{OV}, \lambda) \cdot N_{\text{ph}} \tag{4}$$

The SiPM dynamic response is linear as long as the incident photons are lower than the overall number of device microcells. In fact, since the output pulse of a single cell

is independent of the number of incident photons initiating the avalanche, as the impinging photon rate per microcell increases, the probability that two or more photons will interact within the same pixel at the same time becomes greater. The detector dynamic response begins to become sub-linear when N_{det} approaches N. In other terms, at low optical signal levels, the SiPM photocurrent is proportional to the incident optical power, giving a linear detector response; as the optical power increases, the SiPM photocurrent begins to deviate from linearity and finally saturates due to the limited number of microcell [17].

However, a more recent research has demonstrated how the SiPM response deviation from linearity starts much earlier than the effective number of detected photons becomes comparable to the total number of SiPM microcells [18].

In addition to the afore discussed aspects, which are merely related to the specific SiPM detector, a different kind of linearity should also be paid attention to, which is instead dependent on the particular characterization methodology adopted to achieve PDE measurements, and is thus here addressed.

The incident photon flux rate impinging on the SiPM detector at a specific wavelength is evaluated starting from the measured current produced by the reference photodiode as a result of the effective number of incident photons per unit time. The photon flux rate on the calibrated photodiode is calculated as

$$\Phi_{\mathrm{PhD}}^{\mathrm{inc}} = \frac{I_{s\mathrm{PhD}} - I_{d\mathrm{PhD}}}{q} \cdot \frac{1}{QE_{\mathrm{PhD}}} \tag{5}$$

where $I_{s\mathrm{PhD}}$ and $I_{d\mathrm{PhD}}$ are respectively the measured and dark current of the reference photodiode, QE_{PhD} is its NIST traced quantum efficiency at the same operating wavelength, and q is the elementary electron charge.

Under uniform illumination conditions, the effective incident photon rate on the SiPM detector is derived as

$$\Phi_{\mathrm{SiPM}}^{\mathrm{inc}} = \Phi_{\mathrm{PhD}}^{\mathrm{inc}} \cdot \frac{A_{\mathrm{SiPM}}}{A_{\mathrm{PhD}}} \cdot \Gamma_{\mathrm{f}} \tag{6}$$

where A_{SiPM} and A_{PhD} are the SiPM and reference photodiode sensitive surface areas, respectively, and Γ_{f} is the transmittance of the neutral density filter exploited for attenuating the incident light flux on the SiPM device (see section II).

The effective number of SiPM pulses per second detected by the counter module for a 0.5-pe discriminator threshold is then evaluated in the desired range of wavelengths and bias voltages to obtain the corresponding PDE measurements, according to

$$\Phi_{\mathrm{SiPM}}^{\mathrm{det}} = PDE \cdot \Phi_{\mathrm{SiPM}}^{\mathrm{inc}} \tag{7}$$

where $\Phi_{\mathrm{SiPM}}^{\mathrm{det}}$ represents the measured photon flux rate detected by the sensor in terms of pulse counts per second.

Under low-level illumination (in single-photon regime), the number of pulses detected from the measurement apparatus per unit time increases linearly with the incident photon flux, since the average time between two consecutive detected photons is greater than the recovery time of the single SiPM microcell. On the other hand, as soon as the incident photon rate increases, the number of detected pulse counts begins to deviate from linearity because the probability that two or more photons will trigger the SiPM pixels within their recharging transition becomes higher. Indeed, despite the number of fired cells can be established by the amplitude of the detected pulses, the measurement system at a 0.5-pe threshold cannot distinguish among multiple incident photons within the recovery time of the single diode pixel. This effect thus causes a reduction in the measured PDE and is more pronounced for slow recharging SiPMs.

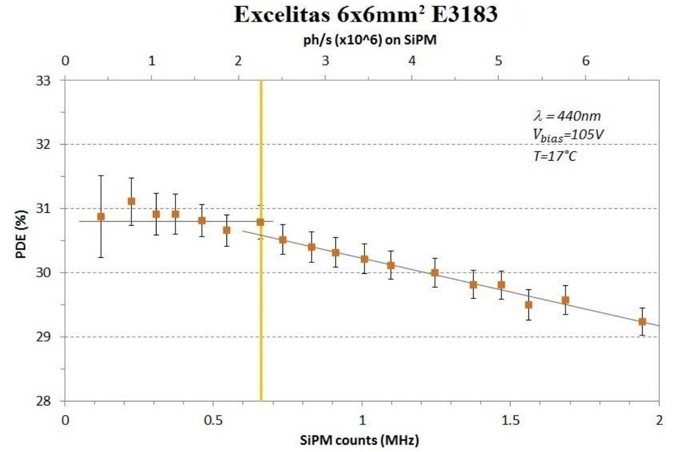

Fig. 9. PDE degradation plot as a function of the incident photon flux for the Excelitas E3183 detector.

Therefore, in order to prevent the SiPM detector from saturation during PDE measurements, preliminary linearity tests have to be carried out for each type of device. In other words, the best illumination conditions should be guaranteed, in such a way to avoid system saturation while maintaining, at the same time, a sufficiently high signal level on the calibrated photodiode.

Photon rate measurements are performed by illuminating the integrating sphere and selecting the desired wavelength.

As an exemplary illustration, Fig. 9 shows the measured PDE values from the Excelitas 6×6-mm^2 detector at $\lambda =$ 440nm as a function of the effective count rate (with the DCR contribution removed), which allows for a proper selection of the appropriate photon rate for the specific device. It appears from this kind of plot how the measured PDE begins to drop off over a given photon counting rate (~650kHz in Fig. 9, corresponding to about 2.25×10^6ph/s in the upper axis), through which the optimum photon flux can be determined to avoid PDE degradation.

D. Photon Detection Efficiency Measurements

Only a fraction of the total number of photons impinging on the SiPM detector actually triggers avalanches and, as a result, a detectable signal. The foremost reasons for such inefficiencies are geometrical (inactive regions between microcells), physical (reflection/absorption by passive layers), and electrical (photon conversion occurring where the electric field is not suitable for triggering the avalanche). The overall efficiency of the sensor is usually referred to as PDE, defined as the statistical probability for an incident photon to generate a Geiger pulse from one of the SiPM microcells, and it

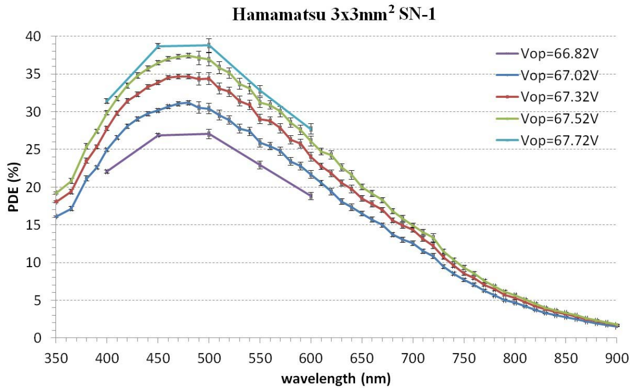

Fig. 10. PDE measurements as a function of wavelength of the Hamamatsu SN-1 detector for different operating voltages.

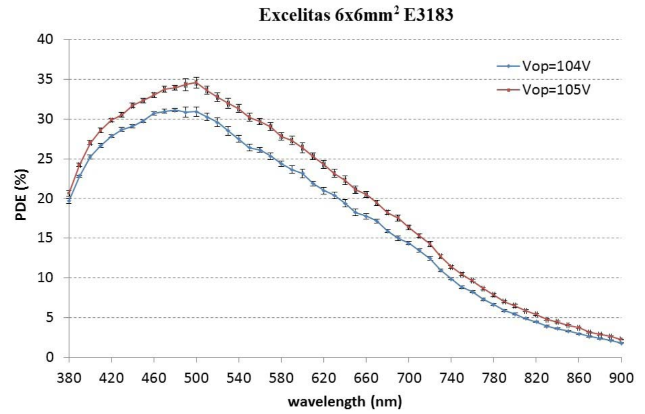

Fig. 11. PDE measurements as a function of wavelength of the Excelitas E3183 detector for different operating voltages.

therefore relates the real number of impinging photons to the measured ones.

More specifically, the SiPM PDE is a function of wavelenght and overvoltage, and is basically determined by

$$PDE\,(V_{OV}, \lambda) = \eta\,(\lambda) \cdot \epsilon\,(V_{OV}) \cdot F \tag{8}$$

where $\eta\,(\lambda)$ is the wavelenght dependent quantum efficiency of silicon, $\epsilon\,(V_{OV})$ is the avalanche initiation probability of charge carriers, and F is the device geometrical fill factor.

The silicon quantum efficiency $\eta\,(\lambda)$ is the probability for an incident photon to generate an electron-hole pair in a region in which carriers can produce an avalanche discharge. The SiPM layer structure is optimized to have the highest probability for a visible photon to be absorbed in the deplection layer. The band gap of silicon puts a superior limit to the operating wavelenghts, while surface reflections and junction depths limit the detection of photons towards the lowest wavelenghts.

The avalanche breakdown probability $\epsilon\,(V_{OV})$ represents the probability that a seed carrier in the deplection region initiates a Geiger discharge, and is a function of the applied bias voltage, since it depends on the impact ionization coefficients of charge carriers, which are strong functions of the electric field.

The geometrical efficiency factor F is defined as the ratio of the total active area of the SiPM microcells to the overall device area, as a result of the gaps among the pixel photodiodes, and is solely determined by the detector topology.

SiPM PDE is commonly calculated from the responsivity of the detector in terms of average photocurrent produced per unit optical power. This method, however, does not account for the noise contributions of cross-talk and afterpulsing, and therefore gives a slight over-estimation of the measured PDE.

SiPM absolute PDE measurements are here performed based on the photon counting method, by which the number of pulses per unit time in monochromatic light conditions are compared to the light level recorded by a reference NIST photodetector at the same time and for several wavelengths.

Fig. 10 and Fig. 11 illustrate the PDE measurements respectively for the Hamamatsu 3×3-mm^2 and Excelitas 6×6-mm^2 detectors over a large wavelengths spectrum and for different operating conditions. Dark noise contributions are removed in both plots. For a given wavelength, PDE values expectedly raise up for greater operating voltages, owing to the higher avalanche breakdown probability ϵ resulting from increased overvoltages in equation (8). However, the PDE behavior begins to saturate (as observable in Fig. 10, where five different PDE curves are reported) when approaching the maximum achievable ϵ.

Of course, dark staircase plots and system linearity measurements described in the previous steps must be repeated before carrying out PDE curves at different overvoltage values.

PDE measurements results for the analyzed detectors do not significantly differ from the datasheet reference values quoted by the manufacturers for a given operating condition.

E. Optical Cross-Talk Measurements

SiPM optical cross-talk occurs when optical photons that are emitted by accelerated charge carriers undergoing an avalanche propagate towards neighboring diode pixels where, depending on their energy and location, they have a certain probability to generate an additional Geiger avalanche discharge; as a consequence, since the original and neighbor avalanches may occur almost simultaneously (on the same scale of few nanoseconds), single absorbed photons may generate output signals equivalent to more than 1-pe avalanche events. Due to the unfeasibility of determining the exact number of photon-induced pixel breakdowns, optical cross-talk may gravely limit the photon-counting resolution of SiPM devices, and the occurrence probability of cross-talk events should thus be considered as one of the major performance parameters of a SiPM detector.

The experimental approach used for assessing the cross-talk probability relies on the analysis of DCR measurement results. For ideal detectors, the probability of two or more simultaneous thermal excitations should be marginal, so that only dark events corresponding to single photoelectrons should be observed. On the other side, in real SiPM sensors, spurious cross-talk induced avalanches can occur resulting in higher amplitude pulses. By comparing the measured event rates above 1-pe threshold with the total dark rate the cross-talk probability is estimated.

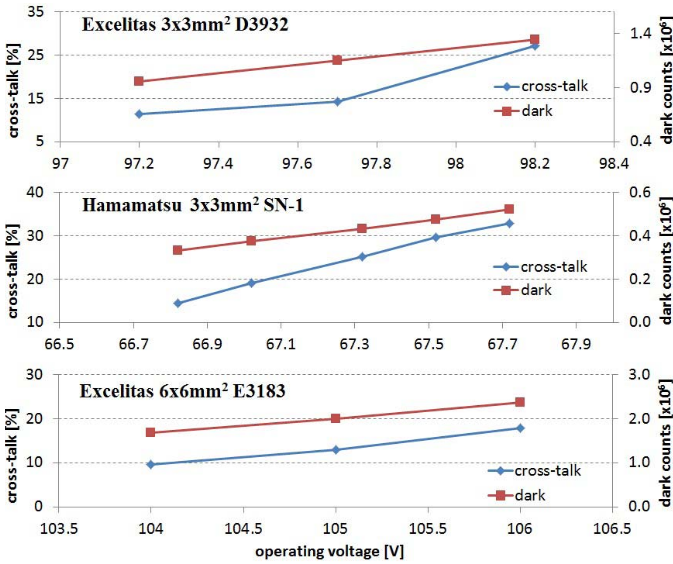

Fig. 12. DCR and cross-talk measurements results of the three analyzed SiPM detectors at different operating voltages.

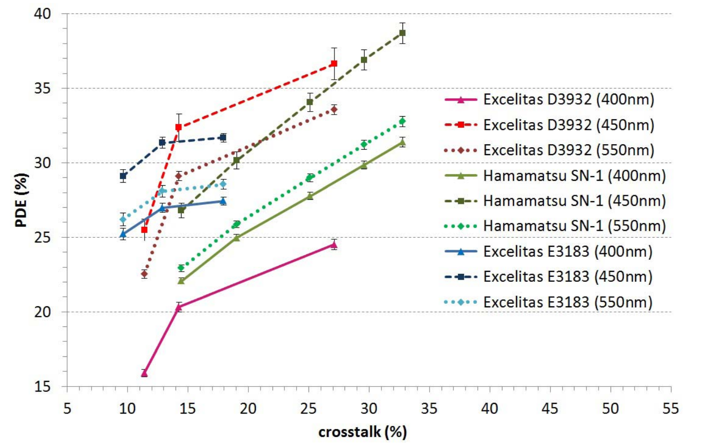

Fig. 13. PDE versus cross-talk measurements of the analyzed SiPM detectors for three different wavelengths at $T = 25$ °C.

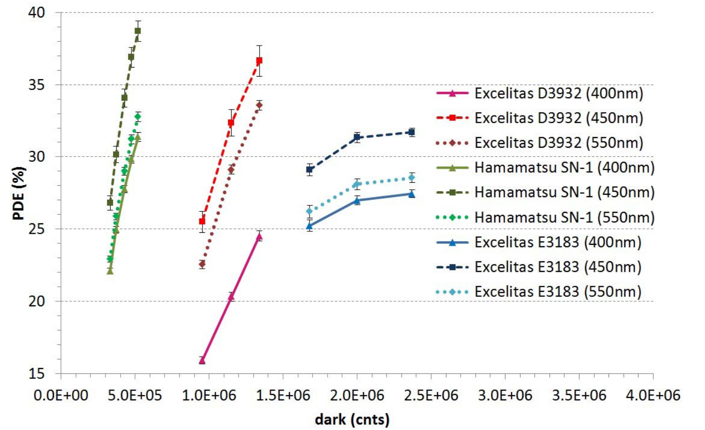

Fig. 14. PDE versus DCR measurements of the analyzed SiPM detectors for three different wavelengths at $T = 25$ °C. The Excelitas E3183 detector shows higher DCR values due to the larger device area.

Optical cross-talk is evaluated from the DCR data as the ratio between the first and the second event count rate. This approach is based on the assumption that the probability of triggering two uncorrelated avalanches within the same rise time is negligible.

The cross-talk functional dependency on the overvoltage is also investigated. Since the number of optical cross-talk events is directly proportional to the amount of charge produced in the avalanche process, which in turn is dependent on the applied overvoltage, the probability of optical cross-talk events is expected to raise up with increasing overvoltage. The occurrence probability of trigger events affected by optical cross-talk increases with the bias voltage as the number of emitted photons increases with the amount of charge carriers flowing during the avalanche discharge.

Cross-talk and DCR measurements results of the three analyzed detectors at different operating voltages are illustrated in Fig. 12, where the rising trends of both parameters are observed.

The cross-talk effect can be significantly reduced by optically isolating the SiPM pixel microcells from each other; this can be accomplished by etching optical trenches among the microcells and filling them with optically opaque materials. Nevertheless, this could involve a considerable fill factor reduction in (8), with possible PDE degradation.

It should here be remarked that optical cross-talk effects are not accounted for in the adopted photon counting technique for determining the detector PDE, as a 0.5-pe threshold is applied to all triggered pulses, such that simultaneous pulses are always measured as a single pulse.

In order to achieve a global comparison among the different SiPM detectors in terms of their most significant performance parameters, and to help choose the optimal operating condition for a specific device, Fig. 13 and Fig. 14 depict the PDE measurements of the analyzed SiPMs at three different wavelengths as a function of cross-talk and dark counts, respectively. Each single data curve in both plots implicitly reflects the cross-talk and DCR functional dependency on the overvoltage, as higher x-axis points for the same detector refer to increased operating voltages. These graphs, carried out at the final step of the SiPM characterization procedure, are believed to be particularly significant and helpful in evaluating the best operating conditions for a particular SiPM detector as a result of an optimal trade-off between PDE and cross-talk, from one side, and PDE and DCR, from the other side; in fact, higher PDE values are obtained at greater overvoltages (before saturation) at the cost of increased cross-talk and DCR. In addition, the above plots can be usefully exploited for comparing the photon detecting capabilities of the characterized SiPMs within the maximum allowed values of the most important noise sources (cross-talk and dark) dictated by the specific application requirements.

It should be here remarked that the three analyzed SiPMs are not actually comparable in terms of DCR, because the Excelitas E3183 detector shows higher dark rates compared to the other devices due to the 4-times greater dimensions.

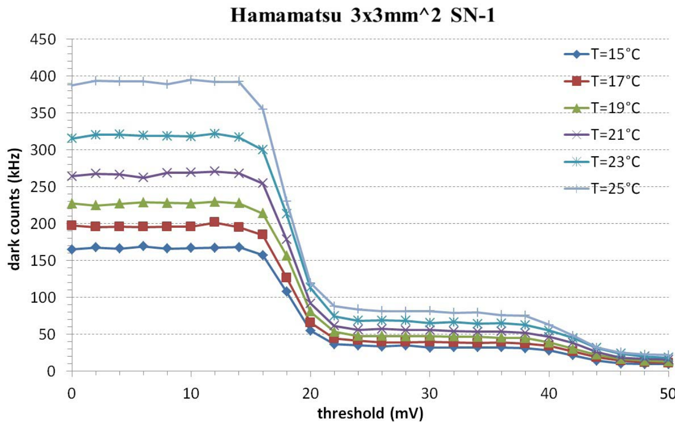

Fig. 15. Dark staircase plots as a function of the discriminator threshold for the Hamamatsu SN-1 detector at different temperature values, for $V_{OV} = 0.88$V.

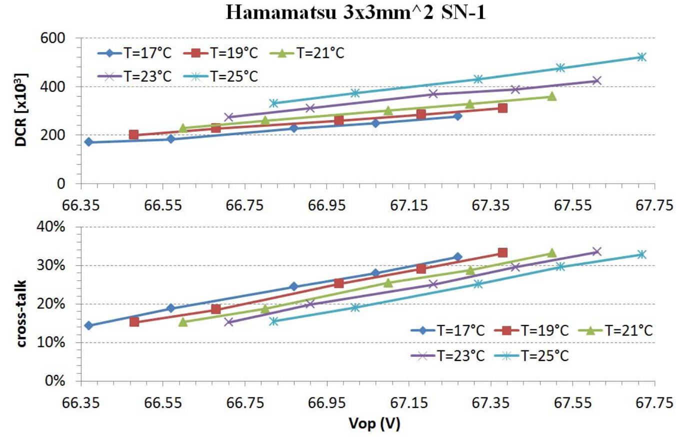

Fig. 16. DCR and cross-talk measurement results as a function of the operating voltage V_{OP} for the Hamamatsu SN-1 detector at different temperature values.

F. Temperature Characterization

It is extremely important that the SiPM operating conditions are maintained as much stable in temperature as achievable for an optimal performance assessment of the detectors under test. Therefore, effective temperature compensation techniques must be devised to obtain reliable measurement results. In addition to the SiPM gain G (which in turn affects the trigger probability ϵ), another important optical parameter is affected by temperature variations, namely the dark count rate.

Based on the thermal coefficient (dV_{BD}/dT) estimation (see part I of the paper), the operating voltage V_{OP} can be effectively compensated with respect to temperature fluctuations to ensure overvoltage stability during temperature measurements.

In the following sets of measures, the SiPM operating temperature T is varied ranging from 15°C to 25°C in steps of 2°C and the dark and cross-talk variations are monitored.

Once the operating temperature is selected and the relevant PSAU compensation activated, DCR stairs should be first performed. Fig. 15 depicts the acquired staircase plots concerning the Hamamatsu SN-1 sensor at a fixed overvoltage value. From the stairs data, DCR and cross-talk contributions can be derived for all analyzed temperatures.

By repeating the same staircase measurements as a function of temperature at different operating conditions and collecting the relevant DCR and cross-talk data for the Hamamatsu device, the comprehensive graphs in Fig. 16 can be obtained, showing the DCR and cross-talk dependencies on the operating voltage at different temperatures. By inspection of the resulting plots, DCR and cross-talk exhibit the expected direct proportionality with V_{OP}, while different trends can be observed as a function of temperature; DCR increases with T, whereas cross-talk does not depend on the operating temperature.

Another way to report the previous results and better outline the temperature dependencies, is to present DCR and cross-talk data values as a function of T for different overvoltages V_{OV}, as illustrated in Fig. 17. Analyzing the above plots, it is found that the DCR contribution approximately halves every 7°C, as expected to occur in silicon devices [19]. Conversely, the cross-talk probability is confirmed to be independent of temperature.

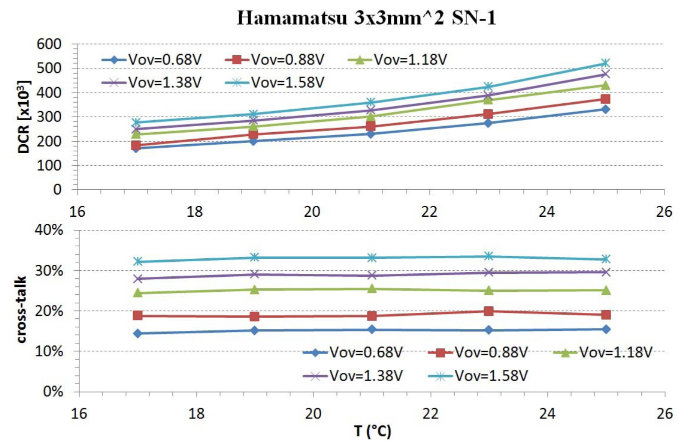

Fig. 17. DCR and cross-talk measurement results as a function of temperature for the Hamamatsu SN-1 detector at different values of the overvoltage V_{OV}. The DCR approximately halves every 7 °C, while the cross-talk probability is almost independent of temperature.

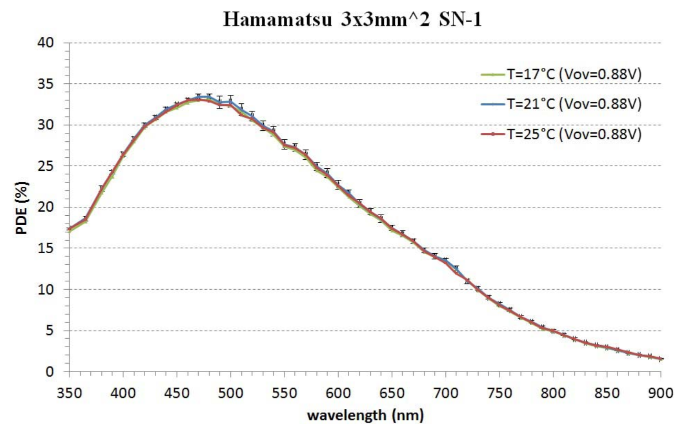

Fig. 18. PDE measurements versus wavelength spectrum for the Hamamatsu SN-1 detector at different temperature values. As expected, no significant PDE variations are obtained as a function of temperature.

Last, as an exemplary case, PDE measurements for the same Hamamatsu detector are also carried out, for a fixed overvoltage and in a large wavelength spectrum, at three different operating temperatures, and the resulting values are presented in Fig. 18. Almost overlapped PDE data curves

are found for all selected temperatures, therefore confirming that SiPM photon detection capabilities are not affected by temperature variations.

IV. Conclusion

A systematic and detailed characterization methodology for SiPM sensors is discussed, with the aim of providing accurate measurements of the most important electro-optical parameters and qualifying the overall device performance. The procedure steps followed and the extensive analyses performed have led to a standardization of the adopted testing methodology, so as to be efficiently applicable to any kind of solid-state detectors. A few recently produced devices are analyzed and their foremost electrical and optical features are estimated, in order to confirm the effectiveness of the envisaged protocols and data-handling procedures in providing a reliable characterization of the SiPM detectors. All evaluated characteristic trends are found to show a good agreement with the expected behavior from the physics theory of the device.

References

[1] P. Finocchiaro *et al.*, "Characterization of a novel 100-channel silicon photomultiplier—Part I: Noise," *IEEE Trans. Electron Devices*, vol. 55, no. 10, pp. 2725–2764, Oct. 2008.

[2] P. Finocchiaro *et al.*, "Characterization of a novel 100-channel silicon photomultiplier—Part II: Charge and time," *IEEE Trans. Electron Devices*, vol. 55, no. 10, pp. 2765–2773, Oct. 2008.

[3] G. Bonanno *et al.*, "Precision measurements of photon detection efficiency for SiPM detectors," *Nucl. Instrum. Methods Phys. Res. A*, vol. 610, no. 1, pp. 93–97, 2009.

[4] M. Petasecca *et al.*, "Thermal and electrical characterization of silicon photomultiplier," *IEEE Trans. Nucl. Sci.*, vol. 55, no. 3, pp. 1686–1690, Jun. 2008.

[5] P. Eckert, H.-C. Schultz-Coulon, W. Shen, R. Stamen, and A. Tadday, "Characterisation studies of silicon photomultipliers," *Nucl. Instrum. Methods Phys. Res. A*, vol. 620, no. 1, pp. 217–226, 2010.

[6] A. Vacheretc *et al.*, "Characterization and simulation of the response of multi-pixel photon counters to low light levels," *Nucl. Instrum. Methods Phys. Res. A*, vol. 656, no. 1, pp. 69–83, 2011.

[7] C. Piemonte *et al.*, "Characterization of the first prototypes of silicon photomultiplier fabricated at ITC-irst," *IEEE Trans. Nucl. Sci.*, vol. 54, no. 1, pp. 236–244, Feb. 2007.

[8] G. Bonanno, M. Belluso, S. Billotta, P. Finocchiaro, and A. Pappalardo, *Photodiodes—World Activities in 2011*, J.-W. Park, Ed. Rijeka, Croatia: InTech, 2011, pp. 247–266.

[9] D. Marano *et al.*, "Improved SPICE electrical model of silicon photomultipliers," *Nucl. Instrum. Methods Phys. Res. A*, vol. 726, pp. 1–7, Oct. 2013.

[10] G. Bonanno *et al.*, "Catania astrophysical observatory facility for UV CCD characterization," in EUV, X-Ray, and Gamma-Ray Instrumentation for Astronomy VII, O. H. Siegmund and M. A. Gummin, Eds., vol. 2808, Proc. SPIE pp. 242–249, Oct. 1996.

[11] M. C. Uslenghi, G. Bonanno, M. Belluso, A. Modica, and P. Bergamini, "Characterization of a photon-counting intensified active pixel sensor (PC-IAPS): Preliminary results," UV/EUV and Visible Space Instrumentation for Astronomy and Solar Physics, O. H. Siegmund, S. Fineschi, and M. A. Gummin, Eds., vol. 4498, Proc. SPIE pp. 185–196, Dec. 2001.

[12] S. Billotta *et al.*, "Characterization of detectors for the italian astronomical quantum photometer project," *J. Modern Opt.*, vol. 52, nos. 2–3, pp. 273–283, 2009.

[13] G. Bonanno *et al.*, "Preliminary test measurements of the SPAD array," in *Scientific Detectors for Astronomy: The Beginning of a New Era*, ser. (Astrophysics and Space Science Library), vol. 300, P. Amico, J. W. Beletic, and J. E. Belectic, Eds. Dordrecht, The Netherlands: Kluwer, 2004, pp. 29–32.

[14] M. Belluso *et al.*, "Characterization of SPAD arrays: First results," in *Scientific Detectors for Astronomy*, vol. 50, J. E. Beletic, J. W. Beletic, and P. Amico, Eds. Berlin, Germany: Springer-Verlag, 2006, p. 469.

[15] E. Sciacca *et al.*, "Silicon planar technology for single-photon optical detectors," *IEEE Trans. Electron Devices*, vol. 50, no. 4, pp. 918–925, Apr. 2003.

[16] D. Marano *et al.*, "Silicon photomultipliers electrical model extensive analytical analysis," *IEEE Trans. Nucl. Sci.*, vol. 61, no. 1, pp. 23–34, Feb. 2014.

[17] M. Grodzicka, M. Moszynski, T. Szczesniak, M. Szawlowski, D. Wolski, and K. Lesniewski, "Effective dead time of APD cells of SiPM," in *Proc. IEEE Nucl. Sci. Symp. Med. Imag. Conf.*, Oct. 2011, pp. 553–562.

[18] L. Gruber, S. E. Brunner, J. Marton, and K. Suzuki, "Over saturation behavior of SiPM at high photon exposure," *Nucl. Instrum. Methods Phys. Res. A*, vol. 737, pp. 11–18, Feb. 2014.

[19] J. R. Janesick, *Scientific Charge-Coupled Devices*. Bellingham, WA, USA: SPIE, 2001.

[20] D. Marano *et al.*, "Accurate analytical single-photoelectron response of silicon photomultipliers," *IEEE Sensors J.*, DOI: 10.1109/JSEN.2014.2316363.

[21] R. Mita and G. Palumbo, "High-speed and compact quenching circuit for single-photon avalanche diodes," *IEEE Trans. Instrum. Meas.*, vol. 57, no. 3, pp. 543–547, Mar. 2008.

Giovanni Bonanno was born in Catania, Italy, in 1955. He received the M.Sc. degree in physics from the University of Catania, in 1980. Since 2001, he has been serving as a Full Astronomer of Astrophysical Technologies with the Osservatorio Astrofisico di Catania, Istituto Nazionale di Astrofisica, Catania. His main research interests and activities include silicon photomultiplier detectors, charge-coupled devices, and photon-counting systems for ground and space astrophysical applications. He is mainly involved in testing, measurements, and characterizations of imaging detectors and related electronic instrumentation. He has co-authored several technical and scientific papers about detectors and electronic controllers for astrophysical applications, and holds one national patent on a photon-counting system. He has been responsible for the design and realization of electronic control systems for the instrumentation of the Italian telescope Galileo (TNG) in La Palma, the stellar site G. Fracastoro on Mount Etna, and some space projects.

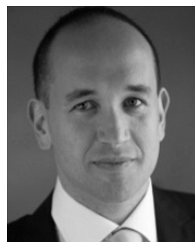

Davide Marano was born in Catania, Italy, in 1979. He received the M.Sc. (*summa cum laude*) degree in electronic engineering from the University of Catania, in 2006, and the Ph.D. degree from the Dipartimento di Ingegneria Elettrica, Elettronica e dei Sistemi, University of Catania, in 2010. Since 2012, he has been with the Osservatorio Astrofisico di Catania, Istituto Nazionale di Astrofisica, Catania, as a Junior Design Engineer. His original research projects have been focused on analog and digital integrated circuits. His main research activities include the design of CMOS high-performance integrated circuits, low-power multistage amplifiers, and high-speed buffers for liquid-crystal display drivers. He has co-authored many scientific papers on mixed electronics.

Massimiliano Belluso was born in Catania, Italy, in 1967. He received the Diploma degree in electronics from the Archimede Institute of Catania, in 1985. In 1987, he joined STMicroelectronics, Catania, as a Junior Designer. From 1992 to 2000, he served as a High-School Instructor of Electronics. Since 2003, he has been with the Osservatorio Astrofisico di Catania, Istituto Nazionale di Astrofisica, Catania, as a Senior Designer of Electronic Systems. His primary research interests include solid-state detectors for astrophysical applications, intensified charge-coupled devices (CCDs), imaging detectors, active pixel sensors, and photon-counting systems. He is mainly involved in the electronic design of CCD controllers and custom electronics using field programmable gate array. He has co-authored several technical and scientific articles, and holds an international and an Italian patent on photon-counting systems.

Sergio Billotta was born in Catania, Italy, in 1976. He received the M.Sc. degree in physics from the University of Catania, in 2003. In 2003, he joined STMicroelectronics, Catania, as a Research Consultant. Since 2004, he has been with the Osservatorio Astrofisico di Catania, Istituto Nazionale di Astrofisica, Catania, as a Full Researcher. His main research interests and activities include single-photon avalanche photodiodes, silicon photomultiplier detectors, charge-coupled devices, active pixel sensors, imaging detectors, and photon-counting systems for ground and space astrophysical applications. He is mainly involved in full electronic testing, measurements, and characterizations of imaging detectors. He has co-authored many technical and scientific papers, and is currently joining interferometer and quantum astronomy programs.

Alessandro Grillo was born in Francavilla di Sicilia, Italy, in 1968. He received the M.Sc. degree in computer science from the University of Catania, in 2005. From 2006 to 2007, he was a Collaborator for the project TriGrid VL (Virtual Laboratory) with the Osservatorio Astrofisico di Catania (OACT), Istituto Nazionale di Astrofisica, Catania, as a System Manager for HPC-Grid systems developing network environments for the Theoretical Virtual Observatory implementation. From 2007 to 2011, he collaborated with Consorzio COMETA, Catania, as a Technologist System Manager for the administration of grid computing and storage systems and the optimization of high-performance computing environments on parallel systems based on Linux cluster. Since 2011, he has been developing software for the control interfaces of laboratory equipment in Java, C, and C++ languages. Within the activities of OACT, he has participated in the development of web science portals, and is listed as a co-author in several scientific publications on specialized topics about computing and ICT.

Salvatore Garozzo was born in Catania, Italy, in 1978. He received the M.Sc. degree in electronic engineering from the University of Catania, in 2004, upon discussing a dissertation on AMOLED display drivers, performed at STMicroelectronics, Catania. In 2010, he was a Construction Supervisor in an electrical systems company. Since 2006, he has been serving as a Professor of Electronics with the Secondary High School. Since 2012, he has been with the Osservatorio Astrofisico di Catania, Istituto Nazionale di Astrofisica, Catania, as a Junior Design Engineer. His main research activities include the analysis and design of analog and mixed-signal integrated circuits. He is involved in the electronic design of high-performance integrated circuits and custom electronics based on field programmable gate array.

Giuseppe Romeo was born in Catania, Italy, in 1976. He received the M.Sc. degree in electronic engineering from the University of Catania, Catania, in 2008, upon discussing a dissertation about output resistance adaptation in CMOS buffer amplifiers and buffers. In 2008, he received the certification of skills in electronic design of integrated circuits from the Dipartimento di Ingegneria Elettrica, Elettronica e dei Sistemi, University of Catania. In 2008, he was a Marketing Category Management Supervisor in Euronics Italy. Since 2009, he has been a Teacher of Electronics and Mathematics in secondary schools. Since 2012, he has been a member of the Osservatorio Astrofisico di Catania, Istituto Nazionale di Astrofisica, Catania, where he is currently a Junior Design Engineer with the Laboratory Characterization of Detectors.

Maria Cristina Timpanaro was born in Catania, Italy, in 1965. She received the Diploma degree in electronics in 1983. In 1989, she received the certification of skills as a specialist in programming microprocessors and controllers from the Centro Regionale Siciliano Radio e Telecomunicazioni. Since 1993, she has been with the Osservatorio Astrofisico di Catania, Istituto Nazionale di Astrofisica, Catania, as an Expert Technician of assembling electronic circuits. She has participated in several professional courses about analog and digital electronics. Her main research interests and activities include silicon photomultiplier detectors, charge-coupled devices, and photon-counting systems. She has co-authored technical and scientific papers about detectors and electronic controllers for astrophysical applications.